Journal of Materials Chemistry A

Accepted Manuscript

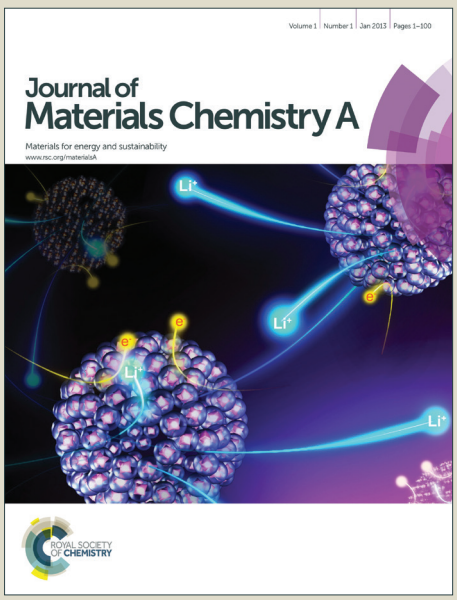

ROYAL SOCIETY OF CHEMISTRY

www.rsc.org/materialsA

Cite this: DOI: 10.1039/c0xx00000x

www.rsc.org/xxxxxx

ARTICLE TYPE

Pentacenequinone derivatives for preparation of gold nanoparticles: Facile Synthesis and Catalytic Application

Kamaldeep Sharma nee Kamaldeep, Sandeep Kaur, Vandana Bhalla,* Manoj Kumar and Ankush Gupta

Received (in XXX, XXX) Xth XXXXXXXXX 20XX, Accepted Xth XXXXXXXXX 20XX

DOI: 10.1039/b000000x

We have designed and synthesized the pentacenequinone/pentacenequinodimethane derivatives **3**, **4** and **6** having nitrile groups using Suzuki–Miyaura coupling and Knoevenagel condensation protocols. Interestingly, these pentacenequinone/pentacenequinodimethane derivatives form fluorescent aggregates in aqueous media due to their aggregation-induced emission enhancement (AIEE) characteristics. Further these fluorescent aggregates generate gold nanoparticles at room temperature without adding any external reducing agent, stabilizing agent and shape-directing additives. In addition, these nanomaterials have been found to have high catalytic activity for the reduction of *p*-nitroaniline to *p*-phenylenediamine.

1. Introduction

Recently, preparation of gold nanoparticles with different morphologies has attracted a lot of research interest[1] due to their size and shape dependent catalytic properties.[2,3] Nanoparticles with high surface to volume ratio act as excellent catalysts in organic reactions.[4] The shape and size controlled catalysis of nitro compounds comparing the catalytic properties of gold nanospheres,[5] gold nanorods,[6] gold nanoprisms[7] and gold nanowires[8] organized into network has been widely investigated and it has been found that gold nanospheres having small size show maximum catalytic efficiency.[4] Thus, it is very important to control the shape of nanoparticles for excellent catalytic efficiency. Among various approaches used for the preparation of gold nanoparticles, wet chemical route is an effective approach for the preparation of gold nanoparticles.[9-14] However, this route suffers from the limitations of longer reaction time and high temperature condition. Further gold nanoparticles of bigger size are generated using this route. Therefore, development of a method for facile and rapid preparation of gold nanoparticles of different morphologies and small size is still a challenge. Recently, we reported aggregates of pentacenequinone derivative which serve as reactors for preparation of palladium nanoparticles.[15] In continuation of this work, we were now interested in development of methods for preparation of gold nanoparticles of different morphologies and hence designed and synthesized novel pentacenequinone/pentacenequinodimethane derivatives **3**, **4** and **6** having nitrile groups. We envisaged that the target molecules may form fluorescent aggregates in aqueous media and presence of nitrile groups will facilitate interaction with gold ions.[16-18] Further, after interaction with fluorescent aggregates, gold ions may be reduced to gold nanoparticles through the compartmentalization mechanism as in case of micellar aggregates.[19] We further envisioned that position of nitrile groups could influence the shape and size of gold nanoparticles. Interestingly, derivatives **3**, **4** and **6** exhibit AIEE characteristics and fluorescent aggregates of these derivatives serve as reactors for preparation of gold nanoparticles. Further, aggregates of derivative **3** can detect gold ions in nanomolar range and reduce gold ions to generate gold nanospheres of size 5-10 nm whereas aggregates of derivatives **4** and **6** generated prisms on reduction of gold ions. To the best of our knowledge, this is the first report where fluorescent aggregates of pentacenequinone/pentacenequinodimethane derivatives having nitrile groups have been used for facile and rapid preparation of gold nanoparticles of different shape and size. Previously, small molecules/polymers having amino group have been used for generation of gold nanoparticles,[9,10,12,13] however, in comparison to those materials, aggregates of pentacenequinone/pentacenequinodimethane derivatives having nitrile groups provide a clean, fast and facile method for preparation of gold nanoparticles of different shape and size (See pS4 in ESI†). Further, the lower limit of detection for the gold ions is better than the limit of detection reported previously in the literature (See pS5 in ESI†). In addition, these nanomaterials have been found to catalyze the chemical reduction of *p*-nitroaniline to *p*-phenylenediamine. The reduction of *p*-

nitroaniline is important as it is widely used in industry because its reduction product, *p*-phenylenediamine, is used in the preparation of azo dyes, fur dyes, polymers, rubber antioxidant and photo developer.[20] The catalytic activity of these nanomaterials is much better than the catalytic activity of the systems reported in literature for this type of reduction (See pS3 in ESI†).

2. Experimental Section

2.1. Materials

All reagents were purchased from Aldrich and were used without further purification. THF was dried over sodium and benzophenone and kept over molecular sieves overnight before use. Silica gel (60–120 mesh) was used for column chromatography.

2.2. Instruments

UV-vis spectra were recorded on a SHIMADZU UV-2450 spectrophotometer, with a quartz cuvette (path length, 1 cm). The cell holder was thermostatted at 25^0 C. The fluorescence spectra were recorded with a SHIMADZU 5301 PC spectrofluorimeter. Scanning electron microscope (SEM) images were obtained with a field-emission scanning electron microscope (SEM CARL ZEISS SUPRA 55). Polarized optical microscope (POM) images were recorded on NIKON ECLIPSE LV100 POL. Elemental analysis (C, H, N) was performed on a Flash EA 1112 CHNS-O analyzer (Thermo Electron Corp.). ^{1}H was recorded on a JEOL-FT NMR–AL 300 MHz spectrophotometer using $CDCl_3$ as solvent and tetramethylsilane $SiMe_4$ as internal standards. UV-vis studies were performed in THF and H_2O/THF mixture. Data are reported as follows: chemical shifts in ppm (δ), multiplicity (s = singlet, d = doublet, br = broad singlet m = multiplet), coupling constants J (Hz), integration, and interpretation.

2.3. Synthesis

Compound 3. To a solution of **1** (0.50 g, 1.07 mmol) and **2** (0.33 g, 2.25 mmol) in 1,4-dioxane (20 ml) were added K_2CO_3 (0.89 g, 6.42 mmol), distilled H_2O (2.10 ml), and $[Pd(PPh_3)_4]$ (0.27 g, 0.24 mmol) under N_2, and the reaction mixture was refluxed overnight. The 1,4-dioxane was then removed under vacuum, and the residue so obtained was treated with water, extracted with dichloromethane, and dried over anhydrous Na_2SO_4. The organic layer was evaporated, and compound was purified by column chromatography using 80:20 (Chloroform: Hexane) as an eluent to give 0.191 g (35%) of compound **3** as yellow solid; mp. >260 ^{o}C; ^{1}H NMR (300 MHz, $CDCl_3$): δ = 7.35 [d, 4H, J = 8.1 Hz, ArH], 7.63 [d, 4H, J = 8.1 ArH], 7.73-7.76 [m, 2H, ArH], 8.14-8.18 [m, 2H, ArH], 8.19 [s, 2H, ArH], 8.98 [s, 2H, ArH]; 9.03 [s, 2H, ArH]; TOF MS ES+: 511.0320; Elemental analysis: Calcd. for $C_{36}H_{18}N_2O_2$: C 84.69; H 3.55; N 5.49 Found: C 84.32; H 3.49 ; N 5.39. Due to poor solubility of compound **3,** its ^{13}C NMR spectrum could not be recorded.

Compound 4. To a solution of **3** (0.50 g, 0.98 mmol) and malononitrile (0.76 g, 19.60 mmol) in 50 ml dry chlorobenzene were added 0.75 ml pyridine and 0.50 ml of $TiCl_4$ under N_2, and the reaction mixture was refluxed overnight. The chlorobenzene was then removed under vacuum, and the residue so obtained was treated with water, extracted with 50 ml of dichloromethane, and dried over anhydrous Na_2SO_4. The organic layer was evaporated, and compound was purified by column chromatography using (80:20) (Chloroform: Hexane) as an eluent to give 0.178 g (30%) of compound **4** as yellowish orange solid; mp: $>260^0$C; ^{1}H NMR (300 MHz, $CDCl_3$): δ = 7.32 [d, 4H, J = 8.1 Hz, ArH], 7.63 [d, 4H, J = 8.7 ArH], 7.78-7.81 [m, 2H, ArH], 8.08-8.10 [m, 2H, ArH], 8.12 [s, 2H, ArH], 8.77 [s, 2H, ArH]; 8.81 [s, 2H, ArH]; ^{13}C NMR (75.45 MHz, $CDCl_3$): 82.31, 112.00, 113.35, 118.23, 126.17, 127.82, 128.70, 129.18, 129.42, 130.40, 130.65, 131.12, 132.31, 132.76, 133.43, 141.09, 143.72, 158.04, 161.18; TOF MS ES+: 629.14 $(M+Na)^+$; Elemental analysis: Calcd. for $C_{42}H_{18}N_6$: C 83.16; H 2.99; N 13.85; Found: C 83.11; H 2.90; N 13.79.

Compound 5. To a solution of **1** (0.5 g, 1.07 mmol) and **2a** (0.72 g, 2.25 mmol) in 1,4-dioxane (20 ml) were added K_2CO_3 (1.18 g, 8.56 mmol), distilled H_2O (3 ml), and $[Pd(PPh_3)_4]$ (0.273g, 0.236 mmol) under N_2, and the reaction mixture was refluxed overnight. The 1,4-dioxane was then removed under vacuum, and the residue so obtained was treated with water, extracted with dichloromethane, and dried over anhydrous Na_2SO_4. The organic layer was evaporated, and compound was purified by column chromatography using 1:1 (Chloroform: Hexane) as an eluent to give 0.248 g (35%) of compound **5** as yellow solid; mp. >260 ^{o}C; ^{1}H NMR (300 MHz, $CDCl_3$): δ = 0.92 [t, 6H, J = 6.6 Hz, $OCH_2CH_2(CH_2)_3\underline{CH_3}$], 1.26 [br, 4H, $OCH_2CH_2CH_2CH_2\underline{CH_2}CH_3$], 1.35-1.37 [m, 4H, $OCH_2CH_2CH_2\underline{CH_2}CH_2CH_3$], 1.48-1.55 [m, 4H, $OCH_2CH_2\underline{CH_2}CH_2CH_2CH_3$], 1.79 [t, 4H, J = 7.35 Hz, $OCH_2\underline{CH_2}(CH_2)_3CH_3$] 3.97 [t, 4H, J = 6.6, $\underline{OCH_2}CH_2(CH_2)_3CH_3$], 6.83 [d, 4H, J = 8.7 Hz, ArH], 7.16 [d, 4H, J = 8.7 ArH], 7.69-7.72 [m, 2H, ArH], 8.09 [s, 2H, ArH], 8.11-8.15 (m, 2H, ArH), 8.94 [s, 2H, ArH], 8.95 (s, 2H, ArH); ^{13}C-NMR δ (75.45 MHz, $CDCl_3$): 14.04, 22.62, 25.76, 29.27, 31.62, 68.04, 99.99, 114.22, 129.47, 129.78, 130.12, 130.60, 130.69, 130.95, 131.14, 132.63, 134.40, 135.27, 142.75, 158.55, 182.94; TOF MS ES+: 685.4335 $(M+Na+2)^+$; Elemental analysis: Calcd. for $C_{46}H_{44}O_4$: C 83.60; H 6.71; Found: C 83.55; H 6.60.

Compound 6. To a mixture of **5** (0.1 g, 0.151 mmol) in 10 ml dry pyridine were added to 0.2 ml of $TiCl_4$ and malononitrile (0.199 g, 3.02 mmol) under N_2, and the reaction mixture was refluxed overnight. After that the reaction mixture was allowed to cool to room temperature. The mixture was then diluted with dichloromethane and washed with water in 2N HCl. The organic layer was separated and dried over anhydrous Na_2SO_4. The solvent was evaporated under reduced pressure to get the crude product. The crude product was purified by column chromatography using 1:1 (Hexane: Chloroform) as an eluent to give 0.246 g (43%) compound **6** as red solid; mp. >260 ^{o}C; ^{1}H NMR (400 MHz, $CDCl_3$): δ = 0.85 [t, 6H, J = 6.0 Hz, $OCH_2CH_2(CH_2)_3\underline{CH_3}$] 1.18 (br, 4H, $OCH_2CH_2CH_2CH_2\underline{CH_2}CH_3$], 1.28-1.29 [m, 4H, $OCH_2CH_2CH_2\underline{CH_2}CH_2CH_3$], 1.40 [br, 4H, $OCH_2CH_2\underline{CH_2}CH_2CH_2CH_3$], 1.72 [t, 4H, J = 8 Hz, $OCH_2\underline{CH_2}(CH_2)_3CH_3$] 3.89 [t, 4H, J = 6 Hz, $\underline{OCH_2}CH_2(CH_2)_3CH_3$] 6.75 [d, 4H, J = 8 Hz, ArH], 7.07 [d, 4H, J = 8 Hz, ArH], 7.68-7.70 [m, 2H, ArH], 7.94 [s, 2H, ArH], 7.98-8.00 [m, 2H, ArH], 8.65 [s, 2H, ArH], 8.68 [s, 2H, ArH]; ^{13}C-NMR δ (75.45 MHz, $CDCl_3$): 13.89, 22.48, 25.62, 29.14, 31.51, 68.06, 81.36, 113.76, 114.40, 126.41, 126.67, 128.70, 129.00, 129.41, 130.43, 130.96, 132.20, 132.58, 133.47, 143.96, 154.62,

158.91, 161.83; TOF MS ES+: 778.5134 $(M + Na)^+$ Elemental analysis: Calcd. for $C_{52}H_{44}N_4O_2$: C 82.51; H 5.86; N 7.40; O 4.23 Found: C 82.46; H 5.80; N 7.36; O 4.20.

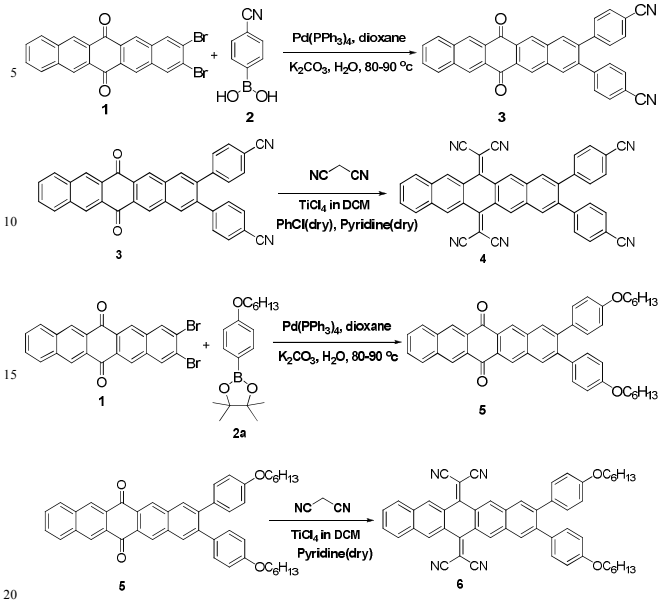

Scheme 1. Synthesis of Pentacenequinone/Pentacenequinodimethane derivatives **3, 4**, **5** and **6.**

3. Results and Discussion

Pentacenequinone derivative **3** was synthesized by Suzuki-Miyaura coupling of boronic acid **2**[21] with 2,3-dibromopentacenequinone **1**,[22] in 35% yield (Scheme1). The structure of derivative **3** was confirmed from its spectroscopic and analytical data. ^{1}H NMR spectrum of derivative **3** showed three singlets at 8.19, 8.99 and 9.04 ppm, two doublets at 7.35 and 7.63 ppm and two multiplets from 7.73-7.76 and 8.14-8.18 ppm, corresponding to the aromatic protons (Fig. S36 in ESI†). The mass spectrum of derivative **3** showed a parent ion peak at m/z 511.0320 $(M+1)^+$ (Fig. S37 in ESI†). These spectroscopic data corroborate the structure **3** for this compound.

The UV-vis spectrum of derivative **3** in THF exhibits an absorption band at 310 nm. On addition of water (≤ 60% volume fractions) to the THF solution of derivative **3**, a new band is observed at 423 nm along with appearance of level-off long wavelength tail (Fig. S1 in ESI†). This new band may be due to intermolecular charge transfer (ICT) state.[23,24] This interaction orginates from the overlapping of pentacenequinone moiety with the nitrile groups of the neighbouring molecule which increases the molecular dipole and ICT state becomes prominent, thus, resulting in formation of a new absorption band (Fig. S1 in ESI†).[24] Further, Mie scattering in the visible region is attributed to the formation of aggregates.[25] The scanning electron microscopy (SEM) image of derivative **3** in the solvent mixture of H_2O/THF (6/4) confirms the presence of interconnected rods (Fig. 1A). The rods formed were visibly transparent and stable at room temperature for several weeks.

The solution of derivative **3** in THF is weakly emissive when excited at 310 nm. However, a dramatic change in fluorescence intensity is observed on addition of water to the THF solution of derivative **3**. On addition of 60% volume fraction of water dual emission at 476 and 562 nm is observed along with enhancement of fluorescence intensity (Fig. 1B).

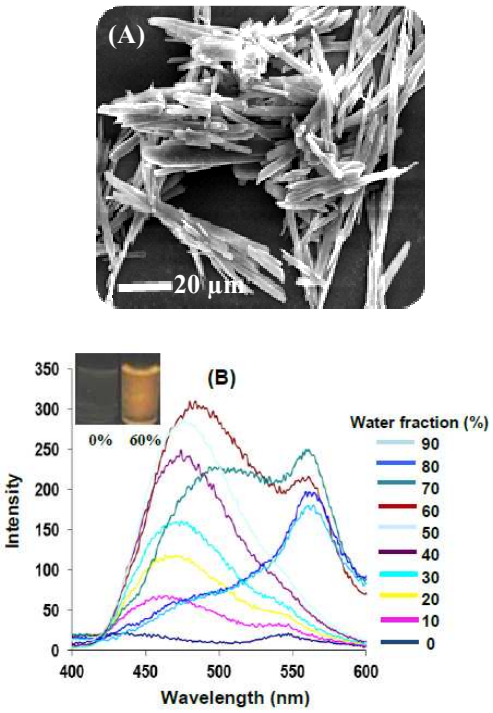

Fig. 1 (A) SEM image of derivative **3** showing the rods in a solvent mixture of H_2O/THF (6/4). Scale bar 20 µm (B) Fluorescence spectra of **3** (10 µM) showing the variation of fluorescence intensity in various H_2O/THF mixtures. Inset photographs (under 365 nm UV light) 0% and 60% water in THF.

The emission maxima at 476 and 562 nm result from locally excited state and intermolecular charge-transfer state, respectively. We believe that head to tail alignment of the molecules (J-aggregation) is responsible for appearance of emission band at longer wavelength (Fig. S2 in ESI†).[26-29] Further, the restriction of intramolecular rotation due to formation of J-aggregates rigidifies the molecule and induces planarization of the molecule, thus, making it more emissive.[29] However, a further increase of water fraction resulted in a decrease in emission intensity (Fig. S3A in ESI†). This phenomenon is often observed in compounds with AIEE properties as after the aggregation only the molecules on the surface of aggregate emit light and contribute to the fluorescence intensity upon excitation, and this leads to a decrease in emission intensity.[30-33] We obtained SEM images of derivative **3** in 60%, 80% and 90% H_2O/THF mixtures and in all cases rods were formed with no significant difference in size (Fig. S3B in ESI†). This shows that the size of the particles do not change on increasing the water fraction, thus, the observed change in the emission behavior may be attributed to the decrease in number of emitting molecules.

Presence of nitrile groups at the periphery of the pentacenequinone core prompted us to investigate its sensing behaviour toward different metal ions by UV-vis and fluorescence spectroscopy. The UV-vis studies of aggregates of derivative **3** (10 µM) in H_2O/THF (6/4) were carried out toward different metal ions such as Cd^{2+}, Ba^{2+}, Hg^{2+}, Fe^{3+}, Ni^{2+}, Zn^{2+},

Cu^{2+}, Pb^{2+}, Ca^{2+}, Co^{2+}, Ag^{+}, Au^{3+}, Na^{+}, K^{+}, Li^{+}, Pd^{2+}, Cr^{3+}, Al^{3+} ions as their perchlorate/chloride/ or both perchlorate and chloride salts (Figs. S5-S6 in ESI†).

Among various metal ions tested aggregates of derivative **3** show selectivity toward Au^{3+} ions (Fig. S7 in ESI†). Upon addition of Au^{3+} ions (50 equiv.) to the solution of derivative **3** in mixed aqueous media (H_2O/THF, 6/4), the absorption band at 305 is red shifted to 318 nm which suggest interaction between aggregates of derivative **3** and Au^{3+} ions (Fig. 2A). A new absorption band is observed at 562 nm which indicates formation of gold nanoparticles (inset Fig. 2A and Fig. S8 in ESI†).[34] The intensity of this band increases with time and the rate constant[35] for the formation of gold nanoparticles was found to be 1.43×10^{-3} sec^{-1} (See pS13 in ESI†).

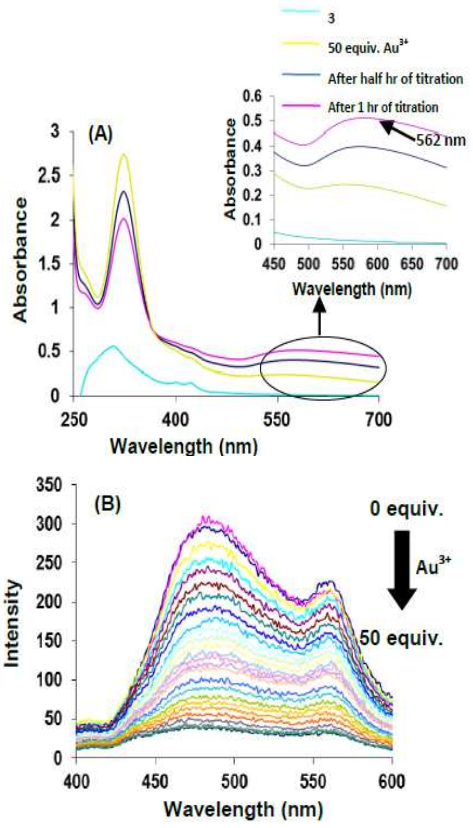

Fig. 2 (A) UV-vis spectra of derivative **3** (10 μM) upon additions of Au^{3+} ions (50 equiv.) and with time in H_2O/THF (6/4) Inset: enlarge UV-vis spectra in range 450-700 nm showing band at 562 nm. (B) Fluorescence spectra of derivative **3** (10 μM) upon addition of Au^{3+} ions in H_2O/THF (6/4); buffered with HEPES, pH = 7.0

There was significant quenching in fluorescence emission upon addition of Au^{3+} ions (0-50 equiv.) to the solution of derivative **3** (H_2O/THF, 6/4) (Fig. 2B). The changes in absorption and emission spectra suggest interaction of gold ions with the nitrile groups of the rods of derivative **3**, and their subsequent reduction to zero valent gold atoms. The calculated detection limit is found to be 100×10^{-9} M for Au^{3+} ions and calculated Stern–Volmer constant of aggregates of derivative **3** for Au^{3+} ions is 5.53×10^{3} M^{-1} (Fig. S10 in ESI†). Under the same conditions as used for Au^{3+} ions, we tested the behaviour of aggregates of derivative **3** toward other metal ions such as Cd^{2+}, Ba^{2+}, Hg^{2+}, Fe^{3+}, Ni^{2+}, Zn^{2+}, Cu^{2+}, Pb^{2+}, Ca^{2+}, Co^{2+}, Ag^{+}, Au^{3+}, Na^{+}, K^{+}, Li^{+}, Pd^{2+}, Cr^{3+} and Al^{3+} ions (Figs. S11-S12 in ESI†) but no significant change in fluorescence intensity was observed except in case of Cu^{2+} and Fe^{3+} ions where 12% and 39% quenching of fluorescence emission was observed, respectively (Fig. S7A in ESI†). Further the aggregates of derivative **3** serve as more sensitive probe for Au^{3+} ions in comparison to other Au^{3+} ion receptors reported in literature (See pS5 in ESI†). To get insight into the mechanism of formation of gold nanoparticles, we slowly evaporated the solution of aggregates of derivative **3** containing gold nanoparticles. After several days, precipitates were observed. The precipitates were filtered and washed with THF. The ^1H NMR of the residue obtained after evaporation of THF solution showed the upfield shifting of aromatic signals (Fig. S13 in ESI†) and its IR spectrum showed a new band at 1725 cm^{-1} attributable to the carbonyl stretching vibrations. Further, the intensity of the band corresponding to –CN group was reduced with a slight shifting (from 2229 to 2227 cm^{-1}) towards lower frequency (Figs. S14-S15 in ESI†). Though we are not able to fully explain the mechanism of reduction yet on the basis of above results we suggest that upon addition of Au^{3+} ions to the solution of aggregates of derivative **3**, the gold ions enter the network of interconnected channels, interact with nitrile moieties[16-18] and get reduced. Thus, aggregates of derivative **3** function as reducing agent as well as stabilizing agent for the preparation of gold nanoparticles.[11,36] We also carried out UV-vis studies of derivative **3** in THF towards Au^{3+} ions. However, absorption spectrum does not indicate formation of nanoparticles (Fig. S16 in ESI†). These studies suggest the importance of water in the preparation of gold nanoparticles.

The polarized optical microscopic (POM) image of the sample containing gold nanoparticles of derivative **3** shows birefringence at room temperature, thus indicating ordered morphology (Fig. S17 in ESI†). The powder X-ray diffraction (XRD) analysis of the sample containing gold nanoparticles of derivative **3** (Fig. S18 in ESI†) showed the characterstic pattern of face-centered cubic (fcc) gold (0).[37]

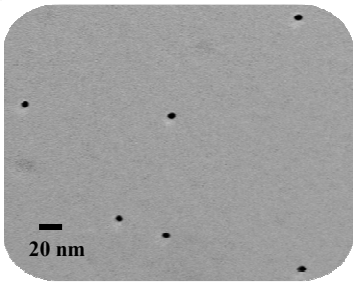

Fig. 3 TEM image of gold nanoparticles of derivative **3**; scale bar 20 nm.

The TEM image of aggregates of derivative **3** in presence of gold ions show the presence of nanospheres (Fig. 3). We also tested generation of gold nanoparticles using 4-Bromobenzonitrile. Upon addition of Au^{3+} ions (50 equiv.) to the solution of 4-Bromobenzonitrile in mixed aqueous media (H_2O/THF, 6/4), no absorption band corresponding to gold nanoparticles was observed in the visible region. However, after allowing the solution to stand for one hour a broad absorption band with weak intensity is observed at 540 nm (Inset Fig. S19 in ESI†).[38] The SEM image of the solution of 4-Bromobenzonitrile in presence of gold ions shows the presence of aggregated spherical gold

nanoparticles (Fig. S20 in ESI†). However, non-aggregated spherical gold nanoparticles are obtained using aggregates of derivative **3** in presence of gold ions (Fig. 3). This study highlights the importance of aggregates of derivative **3** for preparation of non-aggregated gold nanoparticles. To get insight into role of position of nitrile groups, we also prepared pentacenequinodimethane derivatives **4** and **6** (Scheme 1). The Knoevenagel condensation of derivative **3** with malononitrile yield compound **4** in 30% yields. Further, Suzuki-Miyaura coupling of boronic acid **2a**[39] with 2,3-dibromopentacenequinone **1**, yielded compound **5** in 35% yields and its Knoevenagel condensation with malononitrile furnished compound **6** in 43% yield.

The structures of derivatives **4**, **5** and **6** were confirmed from their spectroscopic and analytical data. ^{1}H NMR spectrum of derivative **4** showed three singlets at 8.12, 8.77 and 8.81 ppm, two doublets at 7.32 and 7.63 ppm and two multiplets from 7.78-7.81 and 8.08-8.10 ppm, corresponding to the aromatic protons (Fig. S38 in ESI†). The mass spectrum of derivative **4** showed a parent ion peak at m/z 629.1482 $(M+Na)^+$ (Fig. S40 in ESI†). ^{1}H NMR spectrum of derivative **5** showed one broad signal at 1.26 ppm corresponding to CH_2 groups of hexyl chain, three singlets at 8.09, 8.94 and 8.95 ppm, two doublets at 6.83 and 7.16 ppm corresponding to the aromatic protons, three triplets at 0.92, 1.79 and 3.97 ppm and four multiplets from 1.35-1.37, 1.45-1.55, 7.69-7.72 and 8.11-8.15 ppm due to hexyl chain and aromatic protons, respectively (Fig. S41 in ESI†). The mass spectrum of derivative **5** showed a parent ion peak at m/z 685.4335 $(M+Na+2)^+$ (Fig. S43 in ESI†). Further, ^{1}H NMR spectrum of derivative **6** showed two broad signals at 1.18 and 1.40 ppm corresponding to CH_2 groups of hexyl chain, three singlets at 7.94, 8.65 and 8.68 ppm, two doublets at 6.75 and 7.07 ppm, corresponding to the aromatic protons, three triplets at 0.85, 1.72 and 3.89 ppm and three multiplets from 1.28-1.29, 7.68-7.70, and 7.98-8.00 ppm due to hexyl chain and aromatic protons, respectively (Fig. S44 in ESI†). The mass spectrum of derivative **6** showed a parent ion peak at m/z 778.5134 $(M+Na)^+$ (Fig. S46 in ESI†). These spectroscopic data corroborate the structures **4**, **5** and **6** for these compounds.

UV-visible and fluorescence studies of derivatives **4** and **6** showed that these derivatives form fluorescent aggregates in H_2O/THF mixture due to their AIEE-attributes (Figs. S21-S24 in ESI†).We obtained the SEM images of derivatives **4** and **6** in mixed H_2O/THF solvent mixtures (Figs. S4A-S4B in ESI†). SEM image of aggregates of derivative **4** shows the presence of spherical aggregates in 60% H_2O/THF mixture (6/4) (Fig. S4A (a) in ESI†), however, rod like morphology was observed on increasing water fraction from 60% to 90% (Fig. S4A (b) in ESI†). No significant change in size was observed in case of spherical aggregates of derivative **6** on increasing water fraction from 60% to 90% (Fig. S4B in ESI†). The absorption and fluorescence studies of aggregates of derivatives **4** and **6** (10 μM) were carried out in H_2O/THF toward Au^{3+} ions (Figs. S25-S28 in ESI†) and it was found that aggregates of derivatives **4** and **6** serve as nanoreactors for preparation of gold nanoparticles. The formation of gold nanoparticles is supported by powder XRD and TEM studies (Figs. S29-S31 in ESI†). The TEM image of gold nanoparticles generated by aggregates of derivative **4** show the presence of prisms (Fig. 4A). On the other hand, nanoprisms as well as nanospheres were observed in TEM image of gold nanoparticles generated by aggregates of derivative **6** (Fig. 4B). On the basis of these results, we may conclude that the aggregates of derivative **3** having nitrile groups at periphery form uniform layer around the metal ions and bind strongly with gold ions, hence, rate of reduction is faster (See pS27 in ESI†).[40] This results in greater availability of reduced gold nanoparticles, therefore growth of nanoparticles take place in all the directions leading to formation of nanospheres in case of derivative **3**.[40]

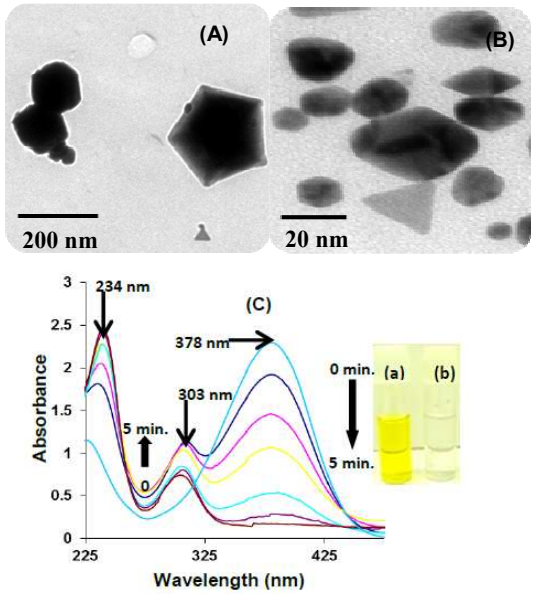

Fig. 4 TEM images of gold nanoparticles of (A) derivative **4** (B) derivative **6**; scale bar (A) 200 nm (B) 20 nm, (C) UV-vis spectra for the reduction of *p*-nitroaniline to *p*-phenylenediamine using gold nanoparticles of derivative **3** as catalyst. Photographs show two different color solutions: (a) yellowish color *p*-nitroaniline; (b) the reduced colorless product *p*-phenylenediamine.

However, in case of derivatives **4** and **6**, nonspherical shape gold nanoparticles were obtained which may be attributed to the non-uniform growth of nanoparticles. We believe that aggregates of pentacenequinodimethane derivatives **4** and **6** form non-uniform layers around the metal ions, thus, resulting in slow reduction of gold ions which is responsible for the formation of gold nanoparticles of non-uniform size.[41]

To check the shape and size dependent catalytic activity of gold nanoparticles, the reduction of *p*-nitroaniline to *p*-phenylenediamine using $NaBH_4$ was investigated (See pS7 in ESI†). The completion of the reaction was confirmed from the color of the solution as well as from the UV-vis spectroscopy. Upon addition of catalytic amount of gold nanoparticles solution 5 µL (2.5 nmol) generated by aggregates of derivative **3** to the solution of *p*-nitroaniline and sodium borohydride, a progressive decrease in the absorbance band at 378 nm and a progressive increase with blue shifting in the absorption band at 234 nm accompanied by appearance of a new absorption band at 303 nm corresponding to *p*-phenylenediamine[42] was observed in five minutes (Fig. 4C). On the other hand, reduction reaction of *p*-nitroaniline to *p*-phenylenediamine using $NaBH_4$ in presence of gold nanoparticles generated by derivatives **4** and **6** took 24

minutes and 18 minutes, respectively (Figs. S33-S34 in ESI†). The calculated rate constants[35] for the catalytic reduction of *p*-nitroaniline by gold nanoparticles of derivatives **3**, **4** and **6** were found to be 1.62×10^{-2} sec^{-1}, 5.64×10^{-3} sec^{-1} and 5.67×10^{-3} sec^{-1}, respectively (See pS27 in ESI†). Thus, gold nanospheres generated by aggregates of derivative **3** exhibit fast catalytic rate due to high availability of active surface area in case of spherical particles.[43] The catalytic efficiency depends upon the available surface area.[44] As the surface area is increased, chances of collisions are also increased and active surface area is maximum in case of nanospheres.[42] The reduction of *p*-nitroaniline was also carried out on large scale. After the complete reduction, the reduced product *p*-phenylenediamine was purified by column chromatography and found to be in 98% yield (Fig. S35 in ESI†). The gold nanoparticles generated by aggregates of derivative **3** exhibit good catalytic efficiency which is even better than that of iron metal catalyzed reduction reported in literature (See pS41 in ESI†).

4. Conclusion

We designed and synthesized AIEE active pentacenequinone/pentacenequinodimethane derivatives **3**, **4** and **6** using Suzuki-Miyaura coupling and Knoevenagel condensation reactions. All the derivatives form fluorescent aggregates in aqueous media due to their AIEE characteristics and selectively detect gold ions. Interestingly, aggregates of derivatives **3**, **4** and **6** serve as reactors for preparation of gold nanospheres and nanoprisms which in combination with $NaBH_4$ smoothly reduces *p*-nitroaniline to *p*-phenylenediamine thus, showing potential application of these nanomaterials in catalysis. The present study demonstrates the influence of position of nitrile groups on morphology and size of nanoparticles.

5. Acknowledgment.

We are thankful to DST (ref. no. SR/S1/OC-63/2010), CSIR (ref. no. 02(0083)/12/EMR-II) and DST-PURSE for financial support. We are also thankful to UGC for awarding university with potential for excellence (UPE) project. S. K. is thankful to DST for INSPIRE fellowship.

6. Notes and references

Department of Chemistry, UGC Sponsored-Centre for Advanced Studies-I, Guru Nanak Dev University, Amritsar-143005, Punjab, India. Fax: +91 (0)183 2258820; Tel: +91 (0)183 2258802-9 ext. 3202; Email vanmanan@yahoo.co.in

† Electronic Supplementary Information (ESI) available: [Optical and spectroscopic data of derivatives **3**-**6**]. See DOI: 10.1039/b000000x/

1 M. Grzelczak, J. P. Juste, P. Mulvaney and L. M. Liz-Marzan, *Chem. Soc. Rev*., 2008, **37**, 1783-1791.
2 N. L. Rosi and C. A. Mirkin, *Chem. Rev*., 2005, **105**, 1547-1562.
3 M. C. Daniel and D. Astruc, *Chem. Rev*., 2004, **104**, 293-346.
4 S. Kundu, S. Lau and H. Liang, *J. Phys. Chem. C,* 2009, **113**, 5150-5156.
5 V. J. Gandubert and R. B. Lennox, *Langmuir,* 2005, **21**, 6532-6539.
6 H-Y. Wu, W-L. Huang and M. H. Huang, *Crystal Growth & Design,* 2007, **7**, 831-835.
7 S. S. Shankar, A. Rai, B. Ankamwar, A. Singh, A. Ahmad and M. Sastry, *Nature Materials,* 2004, **3**, 482-488.
8 S. Kundu, *J. Mater. Chem. C,* 2013, **1**, 831-842.
9 Y. Xia, Y. Xiong, B. Lim and S. E. Skrabalak, *Angew. Chem. Int. Ed.,* 2009, **48**, 60-103.
10 X. Sun, S. Dong and E. Wang, *Angew. Chem. Int. Ed.,* 2004, **43**, 6360-6363.
11 X. Sun, X. Jiang, S. Dong and E. Wang, *Macromol. Rapid Commun.,* 2003, **24**, 1024-1028.
12 X. Sun, S. Dong and E. Wang, *Chem.Commun.,* 2004, 1182-1183.
13 J. A. He, R. Valluzzi, K. Yang, T. Dolukhanyan, C. Sung, J. Kumar and S. K. Tripathy, *Chem. Mater.,* 1999, **11**, 3268-3274.
14 A. M. Alkilany and C. J. Murphy, *Langmuir,* 2009, **25**, 13874-13879.
15 V. Bhalla, A. Gupta and M. Kumar, *Chem. Commun.,* 2012, **48**, 11862-11864.
16 A. Mishchenko, L. A. Zotti, D. Vonlanthen, M. Bürkle, F. Pauly, J. C. Cuevas, M. Mayor and T. Wandlowski, *J. Am. Chem. Soc*., 2011, **133**, 184-187.
17 U. B. Steiner, W. R. Caseri and U. W. Suter, *Langmuir,* 1992, **8**, 2771-2777.
18 N. Tamoto, C. Adachi and K. Nagai, *Chem. Mater*., 1997, **9**, 1077-1085.
19 S. Puvvada, S. Baral, G. M. Chow, S. B. Qadri and B. R. Ratna, *J. Am. Chem. Soc*., 1994, **116**, 2135-2136.
20 X. Bai, Y. Gao, H. Liu and L. Zheng, *J. Phys. Chem. C*, 2009**, 113**, 17730–17736.
21 G. J. Pernıía, J. D. Kilburn, J. W. Essex, R. J. Mortishire-Smith and M. Rowley, *J. Am. Chem. Soc.,* 1996, **118**, 10220-10227.
22 C. R. Swartz, S. R. Parkin, J. E. Bullock, J. E. Anthony, A. C. Mayer and G. G. Malliaras, *Org. Lett*., 2005, **7**, 3163-3166.
23 H. B. Fu, B. H. Loo, D. B. Xiao, R. M. Xie, X. H. Ji, J. N. Yao, B. W. Zhang and L. Q. Zhang, *Angew. Chem. Int. Ed.,* 2002, **41**, 962-965.
24 R. M. Adhikari, B. K. Shah, S. S. Palayangoda and D. C. Neckers, *Langmuir,* 2009, **25***,* 2402-2406.
25 B. Z. Tang, Y. Geng, J. W. Y. Lam, B. Li, X. Jing, X. Wang, F. Wang, A. B. Pakhomov and X. Zhang, *Chem. Mater*., 1999, **11**, 1581-1589.
26 M. Kasha, H. R. Rawls and M. A. El-Bayoumi, *Pure and Applied Chemistry*: IUPAC, Butterworths: London, 1965; vol. **11**, p371.
27 E. G. McRae and M. Kasha, *J. Chem. Phys.,* 1958, **28**, 721-722.
28 E. G. McRae and M. *J.* Kasha, *Physical Processes in Radiation Biology*; Academic Press: New York, 1964; p 23.
29 D. Oelkrug, A. Tompert, J. Gierschner, H-J. Egelhaaf, M. Hanack, M. Hohloch and E. Steinhuber, *J. Phys. Chem. B,* 1998, **102**, 1902-1907.
30 S. Dong, Z. Li and J. Qin, *J. Phys. Chem. B,* 2009, **113**, 434-441.
31 Z. Yang, Z. Chi, B. Xu, H. Li, X. Zhang, X. Li, S. Liu, Y. Zhang and J. Xu, *J. Mater. Chem*., 2010, **20**, 7352-7359.
32 J. Liang, Z. Chen, J. Yin, A. G. Yu and S. H. Liu, *Chem. Commun*., 2013, **49**, 3567-3569.
33 X. Zhang, Z. Chi, B. Xu, C. Chen, X. Zhou, Y. Zhang, S. Liu and J. Xu, *J. Mater. Chem.,* 2012, **22**, 18505–18513.
34 T. Serizawa, Y. Hirai and M. Aizawa, *Langmuir,* 2009, **25**, 12229-12234.
35 S. Goswami, S. Das, K. Aich, D. Sarkar, T. K. Mondal, C. K. Quah and H-K. Fun, *Dalton Trans*., 2013, **42**, 15113–15119.
36 M. N. Nadagouda and R. S. Varma, *Green Chem*., 2008, **10**, 859-862.
37 M. Amin, F. Anwar, M. R. S. A. Janjua, M. A. Iqbal and U. Rashid, *Int. J. Mol. Sci.,* 2012, **13**, 9923-9941.
38 Y. B. Zheng, T. J. Huang, A. Y. Desai, S. J. Wang, L. K. Tan, H. Gao and A. C. H. Huan, *Appl. Phys. Lett.,* 2007, **90**, 183117-3.
39 W. Huang, L. Su and Z. Bo, *J. Am Chem. Soc.,* 2009, **131**, 10348-10349.
40 T. K. Sau and C. J. Murphy, *Langmuir,* 2004, **20**, 6414-6420.
41 M. N. Martin, J. I. Basham, P. Chando and S-K. Eah, *Langmuir*, 2010, **26**, 7410-7417.
42 V. Reddy, R. S. Torati, S. Oh and C. Kim, *Ind. Eng. Chem. Res.,* 2013, **52**, 556-564.
43 R. Fenger, E. Fertitta, H. Kirmse, A. F. Thu¨nemannc and K. Rademann, *Phys. Chem. Chem. Phys.,* 2012, **14**, 9343-9349.
44 A. Roucoux, J. Schulz and H. Patin, *Chem. Rev*., 2002, **102**, 3757-3778.

Graphical Abstract